

https://doi.org/10.1070/QEL17965

Testing the adequacy of a simple theoretical model of dehydration optical clearing of collagen bundles: OCT measurements

O.A. Zyuryukina, M.E. Shvachkina, V.I. Kochubey, Yu.P. Sinichkin, D.A. Yakovlev

Abstract. **Using optical coherence tomography, the scattering coefficients of collagen bundles are estimated at different levels of tissue hydration. We test the validity of a simple theoretical model of dehydration changes in the optical characteristics of a collagen bundle, which is considered as a system of parallel cylinders that model the collagen fibrils forming the bundle. The characteristics of scattering by individual scatterers are calculated using the Mie theory. To take into account the cooperative effects caused by the close packing of the scatterers, use is made of the standard packing function for a system of identical cylinders. The theoretical model also relies on a certain empirical law of changes in the hydration level of fibrils with a change in the water content in the tissue, which predetermines changes in the diameter and refractive index of fibrils during dehydration and rehydration of the tissue. It is shown that the theoretical estimates obtained using this model are in good agreement with the experimental data, which makes it possible to consider this model as reliable.**

Keywords: *light scattering, compression, optical clearing of biological tissues, optical coherence tomography, collagen bundles, fibrils.*

1. Introduction

One of the well-known methods for controlling the optical properties of biological tissues is their mechanical compression. The external pressure applied to a biological tissue changes its morphological and functional state and geometry, the blood volume in blood vessels, and causes the movement of water inside the biological tissue, which affects its optical properties – the ability of the tissue to transmit and reflect light and modify the spectral composition of radiation propagating through the tissue. External compression leads to a change in collimated and diffuse transmission (*in vitro*) and diffuse reflection (*in vitro*, *in vivo*). It reduces diffuse reflection and increases the transparency of biological tissue, which is the result of changes in tissue thickness, density, and optical parameters. Therefore, external compression makes it possible to expand the capabilities of widely and effectively used methods of diffuse reflectance spectroscopy [1] and optical coherence tomography (OCT) of biological tissues [2]. In many cases, for adequate prediction of the effect of mechanical compression, it is necessary not only to know the mechanisms leading to a change in the optical properties of biological tissue, but also to be able to describe this effect at a quantitative level. Despite the fact that the currently available set of theoretical tools used for these purposes is wide and diverse, there is a need for simple methods of description that would allow assessing the effect of compression quickly and accurately.

Compression is often used as a method of optical clearing of biological tissue. Optical clearing of biological tissues increases the depth of light penetration into the tissue and the intensity of light in deeper areas of the tissue, potentially improving the capabilities of various optical, diagnostic and therapeutic methods. The efficiency of clearing depends on the wavelength; therefore, it allows one to estimate the content of chromophores in the tissue, whose absorption under normal conditions is veiled by the absorption of other chromophores and scattering [1, 3]. Optical clearing changes the nature of the transformation of the spectra of radiation propagating from the depth of biological tissue, which should be taken into account when using reflection and luminescence diagnostic methods [4, 5].

Among the mechanisms responsible for the optical clearing of biological tissue during compression, special attention is drawn, as a rule, to the transport of chromophores and the change in the scattering properties of the tissue due to its dehydration. A decrease in light scattering in a compressed biological tissue as a result of its dehydration is the main mechanism of compression optical clearing of dermis, sclera, and other collagen-containing tissues [6, 7]. The present paper is devoted exactly to this mechanism.

The scattering properties of collagen-containing tissues are mainly determined by the optical characteristics of collagen bundles, which consist of collagen fibrils, cylindrical filaments with diameters in the range of 20–500 nm, aligned approximately parallel to each other in the bundle. In the native state, an individual collagen fibril located in the interstitial fluid is a strong scatterer, since its refractive index, despite the large proportion of water in its composition, is significantly higher (by more than 0.1) than that of the surrounding interstitial fluid (the latter is close to the refractive index of water). However, due to the relatively dense packing of fibrils in collagen bundles, the scattering by an ensemble of fibrils due to cooperative interference effects turns out to be much weaker than it could be expected based on the scattering properties of an individual fibril. The role of cooperative effects is most clearly manifested by the eye cornea, which, due to the monodispersity of the system and the quasi-crystalline order of the mutual arrangement of fibrils, hardly scatters light. Unlike the lamellae of the cornea, collagen bundles of the dermis, sclera, tendons and many other tissues as fibril systems are essentially polydisperse – the diameters d_f of the fibrils that make up the bundle can differ by several times (Fig.

O.A. Zyuryukina, M.E. Shvachkina, V.I. Kochubey, Yu.P. Sinichkin, D.A. Yakovlev Saratov State University, ul. Astrakhanskaya 83, 410012 Saratov, Russia; email: saratov_gu@mail.ru, yusin49@gmail.com

Received 2 October 2021
Kvantovaya Elektronika **52** (1) 48–55 (2022)
Translated by V.L. Derbov

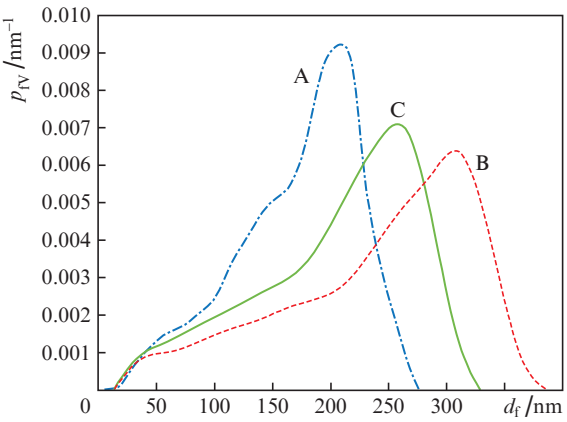

Figure 1. (Colour online) Typical distributions of collagen fibrils by their diameter d_f in tendon bundles [$p_{fV}(d_f)$ is the density of the volume distribution of fibrils; $p_{fV}(d_f)\mathrm{d}d_f$ is the volume portion occupied by fibrils with diameters from d_f to $d_f + \mathrm{d}d_f$, relative to the entire volume occupied by fibrils]. Distributions A and B are constructed according to the experimental data for the samples of the tail tendons of adult rats shown in Fig. 3d [8] and Fig. 2e [9], respectively. In the case of distribution A, the volume average (or mass-average) diameter of fibrils $\bar{d}_f$ is 172 nm; in the case of B, $\bar{d}_f$ = 241 nm; and in the case of C (this is a hypothetical distribution intermediate between distributions A and B), $\bar{d}_f$ = 205 nm.

degree of hydration, defined as the ratio of the volume of water in the system to the volume of the non-aqueous component of the system. The degree of tissue hydration denoted by H means the ratio of the volume of water in the tissue to the volume of the non-aqueous component of the tissue, and the degree of hydration of collagen fibrils H_f is the ratio of the volume of water in the fibrils to the volume of the non-aqueous component of the fibrils. The parameter H is expressed through the volume water content in the tissue c_w as follows: $H = c_w/(1 - c_w)$. The value of the refractive index of fibrils substantially depends on the value of H_f. Within the applicability of the Gladstone–Dahl rule

$$n_f = \frac{n_{dry} + n_w H_f}{1 + H_f}, \tag{1}$$

where n_{dry} is the average refractive index of the non-aqueous component of fibrils, and n_w is the average refractive index of water.

In experiments with collagen-containing tissues (cornea and tendon) [11–13], it was found that at nearly native hydration levels of these tissues, even significant changes in tissue water content do not change H_f significantly. Changes in H_f with a change in H are significant only when H becomes less than a certain critical value. It was shown [14] that in the case of tendons, the available experimental data [11, 14] allow the use of the following approximate dependence $H_f(H)$:

$$H_f(H) = \begin{cases} A_f H, & H \le \dfrac{P_f H_{fn}}{A_f}, \\ H_{fn} - \dfrac{A_f^2}{4H_{fn}(1-P_f)}\left[H + \dfrac{H_{fn}}{A_f}(P_f - 2)\right]^2, & \dfrac{P_f H_{fn}}{A_f} < H \le (2 - P_f)\dfrac{H_{fn}}{A_f}, \\ H_{fn}, & H > (2 - P_f)\dfrac{H_{fn}}{A_f}, \end{cases} \tag{2}$$

1), and in addition, there is no translational ordering in the arrangement of fibrils. Despite this, the role of cooperative effects in the optics of such bundles remains very important, and they significantly determine the changes that occur in the optical properties of collagen-containing tissues during their dehydration [6, 10].

The purpose of this work is to verify experimentally the adequacy of a simple theoretical model for assessing the scattering coefficients of collagen bundles at different levels of tissue hydration. The model is discussed in Section 2. Section 3 describes the experimental technique. It relies on the use of optical coherence tomography to monitor both the degree of tissue hydration and its scattering properties simultaneously. Section 4 presents the main results and their discussion.

2. Theoretical models

As an optical model of a collagen bundle in calculating its scattering characteristics, a polydisperse system of parallel infinite dielectric cylinders with a refractive index n_f, which are models of collagen fibrils, in an isotropic medium with a refractive index n_m, representing an interstitial fluid, is considered. We will assume n_m to be equal to the refractive index of water with good accuracy.

In collagen bundles, water is distributed between the interstitial fluid and the fibrils. The ratio of the volume of water in the fibrils to the volume of water in the interstitial fluid depends on the degree of tissue hydration. In this work, for brevity, we will use the term ‘degree of hydration’ for the volume

where $A_f = 0.9729$, $P_f = 0.1034$, and $H_{fn} = 0.6404$ (Fig. 2a). According to Eqn (2), H_f at $H < 0.07$ changes proportionally to H, A_f being the proportionality coefficient. At $H > 1.25$ (the range that corresponds to the native level of tissue hydration) there is a plateau $H_f(H) = H_{fn}$. The value of the parameter P_f determines the width of the transition zone from the initial linear section to the plateau. The given values of the parameters A_f, P_f, and H_{fn} were determined in Ref. [14] by the least squares method using a large set of experimental points (H, H_f) obtained in the study of the dependence of the birefringence coefficient of collagen bundles on the degree of their hydration. Figures 2b–2e shows an approximate packing of fibrils in a collagen bundle at different levels of tissue hydration. Figure 3 shows how the volume fraction of fibrils in the bundle

$$f_V = \frac{1 + H_f}{1 + H} \tag{3}$$

and the diameter of fibrils d_f change with the water content in the tissue (in accordance with the considered model of tissue hydration). The dependence of the parameter

$$s_d \equiv \frac{d_f}{d_{fn}} = \sqrt{\frac{1 + H_f}{1 + H_{fn}}}, \tag{4}$$

on c_w is presented, which is defined as the ratio of the fibril diameter at a given H to the diameter of the same fibril d_{fn} at a native level of tissue hydration.

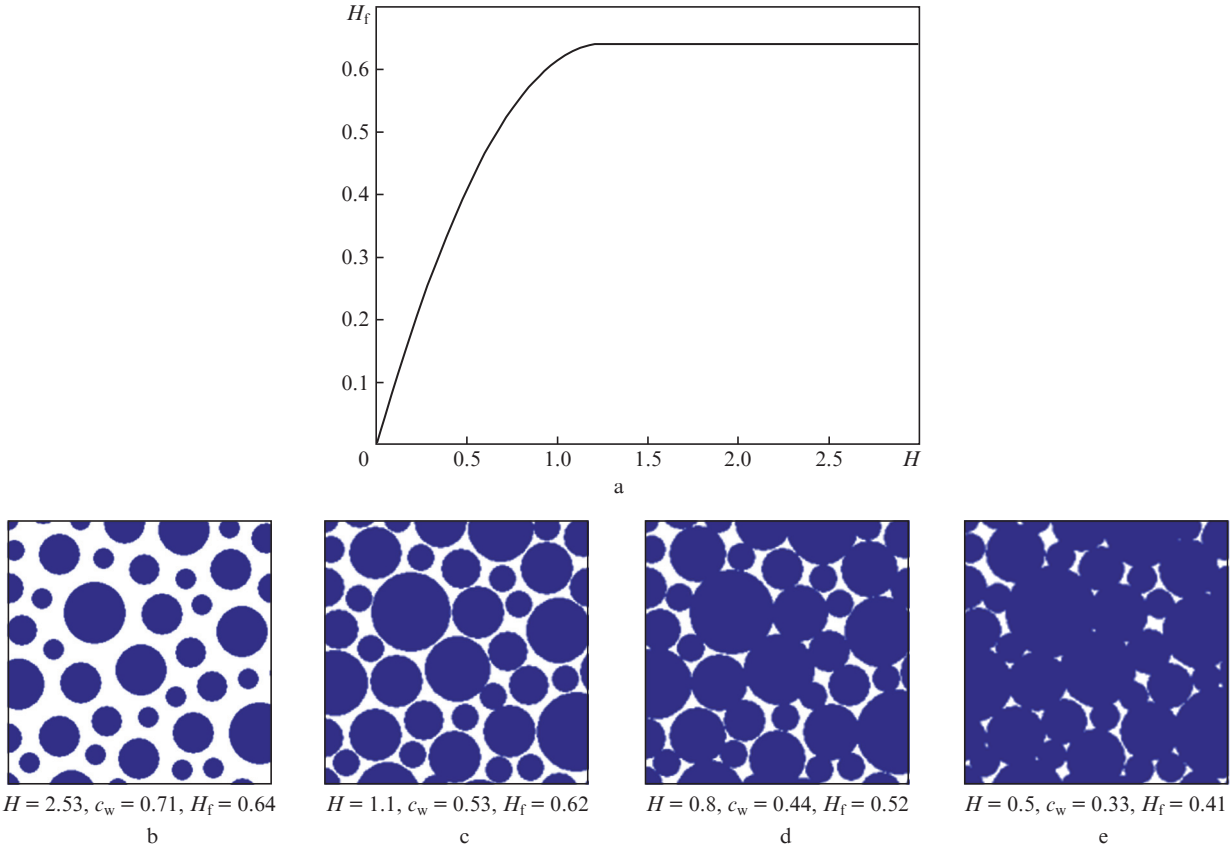

Figure 2. (Colour online) (a) Function $H_f(H)$ given by Eqn (2), and (b–e) the packing of fibrils in the collagen bundle at different levels of tissue hydration at $H_f(H)$ of form (2).

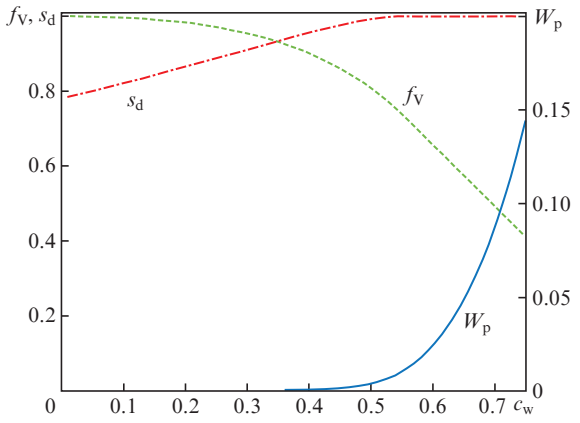

Figure 3. (Colour online) Dependences of the volume fraction of fibrils in the bundle f_V, parameter s_d, and packing factor W_p on the water content in the tissue c_w for the hydration model (2).

When light is incident on a cylinder perpendicular to its axis, the amount and angular distribution of radiation scattered by the cylinder strongly depend on the polarisation state of the incident light (Fig. 4). Due to the orientation ordering of cylinders (fibrils), the same can be said about the scattering of light by the system of cylinders. In this case, the system can be characterised by two principal scattering coefficients, $\mu_{s\|}$ and $\mu_{s\perp}$, for the direction of the incident light polarisation parallel and perpendicular to the axis of the cylinders, respectively. In the model considered, using approximations widely used in biotissue optics [15], the coefficients $\mu_{s\|}$ and $\mu_{s\perp}$ are represented as

$$\mu_{s\|} = \langle\alpha_{V\|}\rangle f_V W_p(f_V), \quad \mu_{s\perp} = \langle\alpha_{V\perp}\rangle f_V W_p(f_V), \tag{5}$$

where $\langle\alpha_{V\|}\rangle$ and $\langle\alpha_{V\perp}\rangle$ are the average volume scattering coefficients of fibrils (cylinders) calculated for a given fibril size distribution [see Eqns (7)]; and W_p is the packing factor that takes into account cooperative effects [15, 16]. In this paper, we will use the packing function $W_p(f_V)$ of the form [15, 16]:

$$W_p = \frac{(1-f_V)^3}{1+f_V}. \tag{6}$$

Formula (6) was derived for an ensemble of identical cylinders [16]. When considering polydisperse systems, as in our case, it is used as an approximation. The dependence of W_p on c_w, corresponding to Eqns (2) and (6), is shown in Fig. 3.

The parameters $\langle\alpha_{V\|}\rangle$ and $\langle\alpha_{V\perp}\rangle$ are calculated by the formulae

$$\langle\alpha_{V\|}\rangle = \frac{2}{\pi}\int\frac{Q_{s\|}(d)}{d}p_{fV}(d)\,\mathrm{d}d,$$
$$\langle\alpha_{V\perp}\rangle = \frac{2}{\pi}\int\frac{Q_{s\perp}(d)}{d}p_{fV}(d)\,\mathrm{d}d, \tag{7}$$

where $Q_{s\|}(d)$ and $Q_{s\perp}(d)$ are the scattering efficiency factors for a cylinder of diameter d for the incident light with

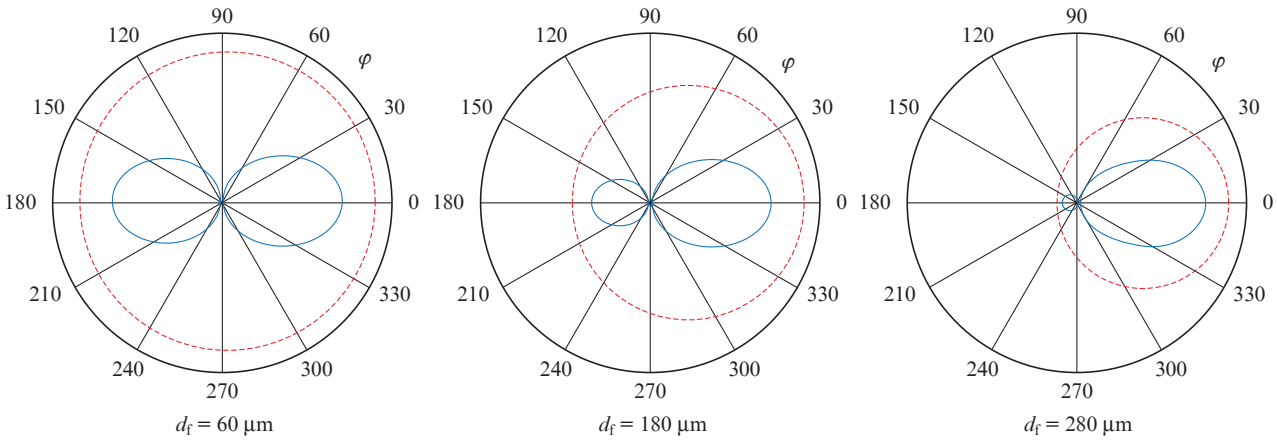

Figure 4. (Colour online) Scattering indicatrices of cylinders of different diameters d_f for light linearly polarised parallel (dashed curve) and perpendicular (solid curve) to the cylinder axis. Light with a wavelength of 930 nm is incident on the cylinder perpendicular to its axis. The refractive index of the cylinder material is n_f = 1.485 (fibrils in the native state); n_m = 1.325 (water); φ (deg) is the scattering angle.

the polarisation direction parallel and perpendicular to the cylinder axis, respectively; and $p_{fV}(d)$ is the distribution of cylinders (fibrils) by diameter (see Fig. 1). The factors $Q_{s\parallel}$ and $Q_{s\perp}$ can be calculated rigorously according to the well-known formulae of the Mie scattering theory for cylinders. For these purposes, we used the BHCYL procedure presented in monograph [17]. As an example, Fig. 5 shows the dependences of $\langle\alpha_{V\parallel}\rangle$ and $\langle\alpha_{V\perp}\rangle$ on c_w for three fibril size distributions (A, B, and C) shown in Fig. 1 (they are taken to characterise the size of fibrils in the native state), calculated for the following parameters: λ = 930 nm, n_{dry} = 1.587, and $n_m = n_w$ = 1.325 (water) [18]. The estimate n_{dry} = 1.587 agrees with the experimental extrapolation value of the group refractive index of collagen bundles at $c_w = 0$ $n_{dry(g)}$ = 1.594 obtained in Ref. [19] (see also Ref. [20]). The value 1.587 is obtained for n_{dry} using the formula

$$n_{dry} = n_{dry(g)} + \lambda \frac{dn_{dry}}{d\lambda}\bigg|_{\lambda = 930\ nm}.$$

The second term was estimated using the data of Ref. [21] for the refractive index of gelatine (see [19]). Figure 5 clearly shows a tendency towards an increase in $\langle\alpha_{V\parallel}\rangle$ and $\langle\alpha_{V\perp}\rangle$ with an increase in the average diameter of fibrils in the tissue.

Figure 6 shows the calculated dependences of the scattering coefficients $\mu_{s\parallel}$ and $\mu_{s\perp}$ corresponding to distributions A, B, and C on c_w. The form of dependences $\mu_{s\parallel}(c_w)$ and $\mu_{s\perp}(c_w)$ is determined mainly by the nature of the dependence of W_p on c_w (see Fig. 3). Since W_p is small in the range $c_w < 0.4$, the coefficients $\mu_{s\parallel}$ and $\mu_{s\perp}$ are also very small, i.e., according to this model, at $c_w < 0.4$, regardless of the size distribution of fibrils, the tissue should be practically transparent. In the range $0.4 < c_w < 0.75$ (values $c_w > 0.75$ are achieved only in the lamellae of the eye cornea, which are not considered here) $\mu_{s\parallel}$ and $\mu_{s\perp}$ increase monotonically with increasing c_w. At the same time, as seen from Fig. 6, with a larger average fibril diameter higher values of $\mu_{s\parallel}$ and $\mu_{s\perp}$ are achieved for any fixed level of hydration. The ratio $\mu_{s\parallel}/\mu_{s\perp}$ in the region of the $H_f(H)$ plateau ($c_w > 0.56$) does not change when c_w changes and is 2.51 for distribution A, 2.36 for distribution C, and 2.17 for distribution B.

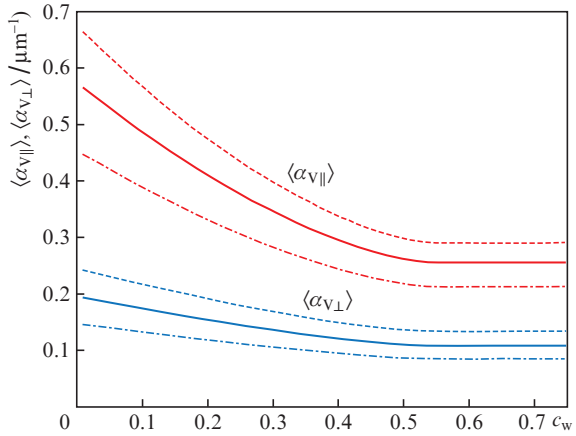

Figure 5. (Colour online) Scattering coefficients $\langle\alpha_{V\parallel}\rangle$ and $\langle\alpha_{V\perp}\rangle$ calculated for the distributions A (dash-dotted curves), B (dashed curves), and C (solid curves).

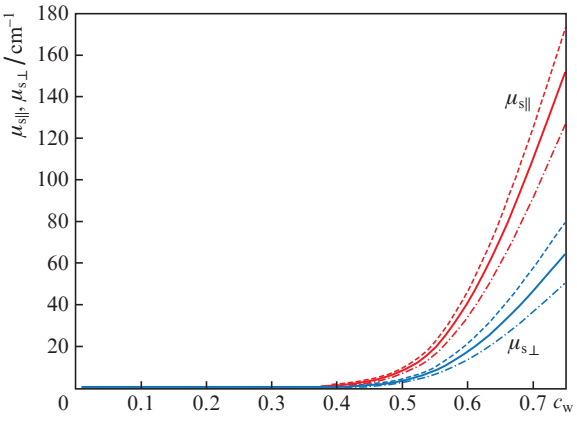

Figure 6. (Colour online) Scattering coefficients $\mu_{s\parallel}$ and $\mu_{s\perp}$ calculated for distributions A (dash-dotted curves), B (dashed curves), and C (solid curves).

The experimental verification of the adequacy of such an assessment of the scattering coefficients of collagen bundles was the main task of this work.

When describing the optical part of the model, for the sake of brevity, we ignored the possible absorption of light in fibrils and interstitial fluid. In the context of this work, this is justified by the fact that in the spectral range where the optical probing of the samples was carried out, the absorption of light in the fibrils and the interstitial fluid filling the space between the fibrils is very small; if necessary, absorption is easy to take into account. Considering the presence of other components in the interstitial fluid, in addition to water, is also not difficult. In the range of c_w values of practical interest, this leads to minor changes in the theoretical curves.

3. Experiment

In this work, both the water content in collagen bundles and their scattering coefficients were estimated using optical coherence tomography. For measurements, we used a spectral-domain tomograph ThorLabs-OCP930SR (the centre wavelength of the probe radiation is $\lambda_0 = 930$ nm, and the bandwidth is 100 nm).

Secondary collagen bundles of rat tail tendons were taken as samples. The structure and composition of the primary collagen bundles (fibres), which make up the secondary tendon bundles, are similar to the structure and composition of collagen fibres of the sclera, dermis, blood vessel walls, heart valve leaflets, etc. The structure of secondary collagen tendon bundles is well studied; it is described in detail in Refs [22–24]. The mass content in tendons in their natural state is usually 24%–38% for collagen and 55%–72% for water [22, 25, 26]. Secondary tendon bundles, the typical diameter of which is 250–500 μm, are tens of times thicker than collagen bundles in other types of tissues, which makes them very convenient for experiments. Due to their relatively simple structure and accessibility, the secondary tendon bundles of the rat tail are a very popular model object for studying the physical and physiological properties of collagen fibres and collagen-containing tissues. In an unloaded state, secondary collagen bundles are characterised by a wavy course of fibres, while closely spaced fibres run parallel to each other. After stretching the bundle by 3%–4%, the orientation of the fibres in it becomes almost uniform. In its structure, the stretched tendon bundle almost ideally corresponds to the optical model of the collagen bundle as a system of parallel cylinders–fibrils (see Section 2), which allows estimating the scattering coefficients $\mu_{s\parallel}$ and $\mu_{s\perp}$.

The diameter of the tendon bundles used in the experiment, taken from adult rats, ranged from 300 to 450 μm. Until the moment of measurements, the samples were kept in normal saline solution (0.9% sodium chloride aqueous solution) for no more than 7 days.

Before the start of measurements, the polarisation of the probe radiation was set parallel to the B-scan plane and did not change during the experiment. Before measurements, the collagen bundle under study, being in saline, was slightly stretched and clamped onto a slide (see Ref. [20]). Then the bundle, immersed in saline solution, was covered with a cover slip and slightly pressed down by it to create large areas of optical contact of the tissue with both the slide and cover slip ($\mu_{s\parallel}$ and $\mu_{s\perp}$ were estimated in such regions). After that, part of the saline solution was removed from under the cover slip using filter paper. Then the sample (collagen bundle) was installed in the OCT-system so that its axis was perpendicular to the B-scan plane, and a scan of the bundle cross section was recorded. The scans obtained with this sample position (position 1, Fig. 7) were subsequently used to estimate the water content in the tissue and the coefficient $\mu_{s\perp}$. Then the sample was rotated by 90° so that the bundle axis was parallel to the B-scan direction, and scans were recorded with this position of the sample (position 2, Fig. 7). These scans were used to estimate the coefficient $\mu_{s\parallel}$. For illustration, Fig. 7 shows OCT images of one of the samples in positions 1 and 2 at a tissue hydration level close to the native one. During two hours at regular intervals (as water evaporated from the saline solution and the tissue became more and more dehydrated), the procedure was repeated. As an example, Fig. 8 shows a series of OCT images of one of the samples in position 1, obtained in this way.

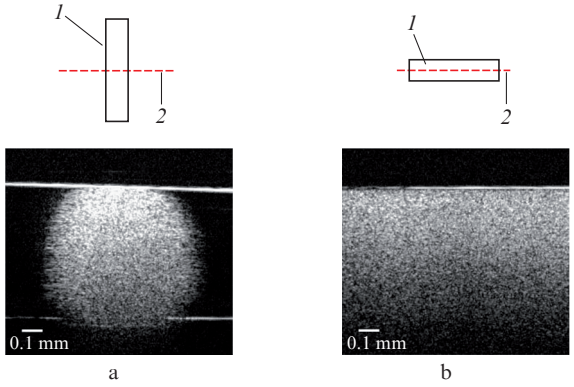

Figure 7. (Colour online) OCT images of a sample of the secondary tendon bundle in positions (a) 1 and (b) 2: (*1*) sample; (*2*) B-scan plane.

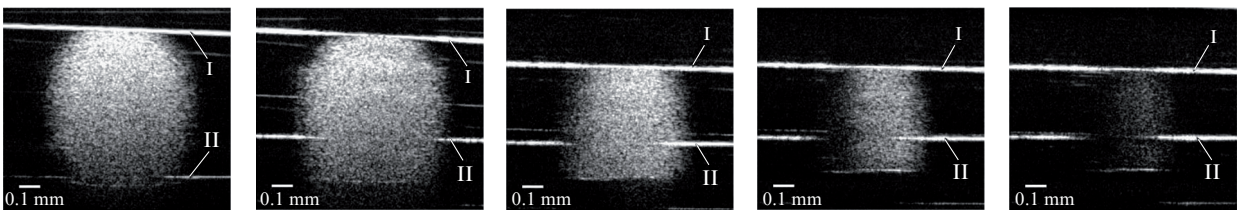

Figure 8. OCT images of a tendon bundle sample in position 1 at different stages of the experiment (labels I and II mark the images of the lower boundary of the cover slip and the upper boundary of the slide, respectively).

The water content in the tissue c_w in the probing region was estimated from the values of the average group refractive index of the tissue $n_{t(g)}$ found from the scans of the sample at position 1. To calculate c_w, we used the formula

$$c_w = \frac{n_{dry(g)} - n_{t(g)}}{n_{dry(g)} - n_{w(g)}} \quad (8)$$

with $n_{w(g)} = 1.341$ (group refractive index of water at a wavelength $\lambda = 930$ nm) and $n_{dry(g)} = 1.594$ (extrapolation value of the group refractive index of the collagen bundle at $c_w = 0$) [14, 19, 20]. The group refractive index of the tissue $n_{t(g)}$ was determined from the shift of the image of the upper boundary of the slide under the sample relative to its position in the absence of the sample; the method for determining $n_{t(g)}$ is described in detail in [14, 19, 20].

The scattering coefficients were estimated from the curves of the dependence of the corrected average OCT signal amplitude on the, calculated as follows [27]:

$$A_c(z) = \frac{\langle A(z)\rangle - \langle A_{dark}(z)\rangle}{\sqrt{t(z - z_f)h(l_{opt}(z))}}, \quad (9)$$

where z is the spatial coordinate in the A-scan direction, measured from the frontal boundary of the sample; $A(z)$ is the amplitude of the OCT signal (brackets $\langle\ \rangle$ denote averaging over adjacent A-scans); $\langle A_{dark}(z)\rangle$ is the average amplitude of the background signal measured in the absence of a sample in the object arm of the interferometer; $t(z - z_f)$ is the function that takes into account the confocal nature of the optical probing system [28]; z_f is the coordinate of the plane of the probe beam waist in the region of its propagation inside the sample; $h(l_{opt}(z))$ is a function that describes the decrease in sensitivity with increasing distance from the plane of zero delay of the interferometer to the probed point, which is characteristic of spectral OCT systems and is due to the finite spectral resolution of the spectrometer of the OCT system [29]; and $l_{opt}(z)$ is the optical path length from the plane of zero delay of the interferometer to the current probed point, the position of which is characterised by the coordinate z. The parameters of the functions $t(z - z_f)$ and $h(l_{opt}(z))$ were determined experimentally as a result of calibration measurements with a planar diffuse scatterer as a sample. All measurements were carried out at the same focusing of the probing system, i.e. the position of the waist of the probing beam incident on the cover slip was fixed. It was determined during calibration measurements. The position of the waist plane of the probe beam in the region of its propagation inside the sample was calculated from the position of the waist of the beam incident on the cover slip using the ABCD rule [30]. When calculating the coordinate z for the points of the A-scan, the value of the average group refractive index of the tissue measured by the above method was used.

To estimate the scattering coefficients, we used the single-exponential approximation [27]

$$A_c(z) \approx A_{c0}\exp(-\mu_{OCT}z). \quad (10)$$

Coefficients μ_{OCT} and A_{c0} were found using the least squares method. It was shown [31] that the value of μ_{OCT} obtained using approximation (10) is close to the value of the corresponding scattering coefficient of the medium if this scattering coefficient does not exceed 60 cm^{-1}. An exception is the cases when the scattering indicatrix of the medium is narrow ($g > 0.8$) [32–34]. In our case, the scattering indicatrices for both polarisations of the incident light are wide (see Fig. 4).

The reliability of this technique for evaluating scattering coefficients was confirmed by the results of test measurements carried out on a layer of *Intralipid*® 20% suspension diluted with distilled water in a ratio of 1:16 by volume. According to the literature data [35], at such a concentration of intralipid, the scattering coefficient of the suspension μ_s at a wavelength of 930 nm should be equal to 22.8 cm^{-1}. The value of μ_{OCT} obtained by us was 21 cm^{-1}, i.e., it turned out to be quite close to the above value of μ_s.

In experiments on collagen bundles, the μ_{OCT} values obtained for the sample at position 1 were considered as estimates for $\mu_{s\perp}$, and the values obtained at position 2 as estimates for $\mu_{s\parallel}$.

4. Results and their discussion

Figure 9 shows the main measurement results, namely, the values of μ_{OCT} obtained at different levels of tissue hydration for two orthogonal polarisations of the incident light on six samples of collagen bundles. The data corresponding to position 1 of the sample (when the incident light is polarised perpendicular to the direction of the fibrils) are shown in Fig. 9a;

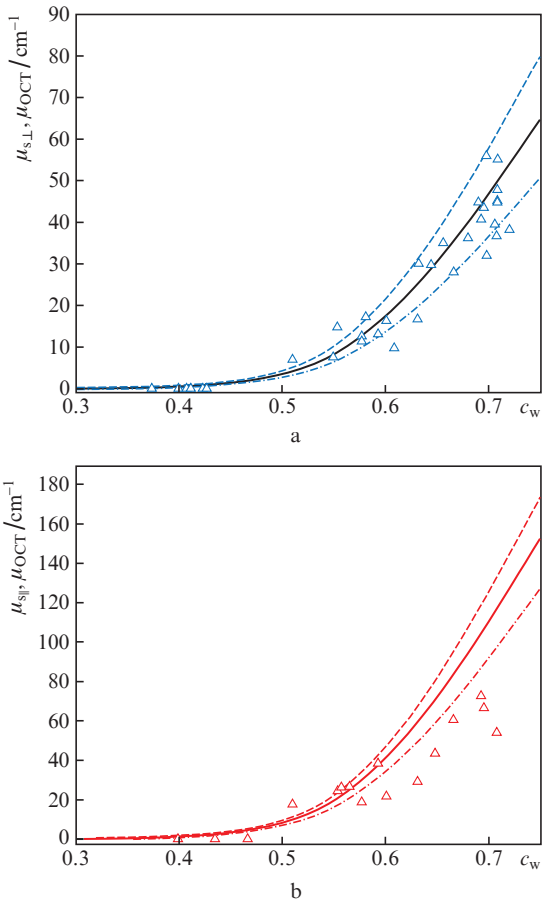

Figure 9. (Colour online) (a) Theoretical dependences $\mu_{s\perp}(c_w)$ and experimental points (c_w,μ_{OCT}) obtained for samples in position 1, and (b) theoretical dependences $\mu_{s\parallel}(c_w)$ and experimental points (c_w,μ_{OCT}) for samples in position 2 (dash-dotted curves – distribution A, dashed curves – distribution B, and solid curves – distribution C).

the data for position 2 (when the direction of polarisation of the incident light is parallel to the direction of the fibrils) are shown in Fig. 9b. For comparison, these figures also show the corresponding theoretical curves from Fig. 6.

The experiment confirmed that for $c_w < 0.4$ and near this region, the scattering in collagen bundles is very weak. In this range of c_w values and up to $c_w = 0.47$, the OCT signal from the sample volume was at the background level, i. e., the scattering was so weak that it did not appear at all in the OCT scans.

As can be seen from Fig. 9a, in the case of polarisation orthogonal to the direction of the fibrils, the experimental data are in good agreement with the theoretical ones over the entire considered range of c_w values. If we assume that the size distributions of fibrils in the samples under consideration are close to distribution C (see Fig. 1) or, varying from sample to sample, are intermediate between distributions A and B, which is quite plausible, we can state a good quantitative agreement between the theoretical and experimental data.

For polarisation parallel to the direction of fibrils (Fig. 9b), good quantitative agreement between the experimental values of μ_{OCT} and theoretical values of $\mu_{s||}$ can be stated only in relation to the range $c_w < 0.6$. In the range $c_w > 0.6$, all experimental points (c_w, μ_{OCT}) lie below the curves $\mu_{s||}(c_w)$ for all three distributions. However, this does not give grounds to assert that the model under consideration gives imprecise estimates in this range: there are signs indicating that in this range the values of μ_{OCT} obtained using approximation (10) should be lower than the true values of $\mu_{s||}$.

Figure 10 shows OCT images of a cross section of a collagen bundle sample in the same position, the first image being recorded with the polarisation of the incident radiation perpendicular to the direction of the fibrils, the second one – with the polarisation of the incident radiation parallel to the direction of the fibrils. The water content in the sample is close to native. It is noteworthy that in the second image, in contrast to the first one, the lower boundary of the collagen bundle is not visible and a long, pronounced haze plume stretches under its image. The presence of such a plume indicates a significant contribution of multiple scattering to the OCT signal [36]. In this case, the absence of the lower boundary of the sample in the image indicates that the OCT signal from the tissue region located at this boundary is formed almost completely due to multiple scattering. It is clear that because of an increase in the level of the OCT signal from great depths due to multiple scattering, the μ_{OCT} values obtained using approximation (10) will be less than the true values of $\mu_{s||}$. The difference in the contributions of multiple scattering to the OCT signal in the two considered situations is obviously related to the fact that $\mu_{s||}$ in the considered region is significantly larger than $\mu_{s\perp}$, and to the difference in the shape of the scattering indicatrices for the considered pair of polarisation states of the incident light (see Fig. 4). Note also that, according to the presented theoretical data, in the case of distribution C, the coefficient $\mu_{s||}$ exceeds the critical level of 60 cm^{-1} [31] at $c_w \approx 0.63$, and the coefficient $\mu_{s\perp}$ at $c_w \approx 0.74$. With the exception of the notoriously unreliable experimental estimates of $\mu_{s||}$ in the region $c_w > 0.6$, all other data obtained in the presented experiment are in good agreement with the theoretical ones.

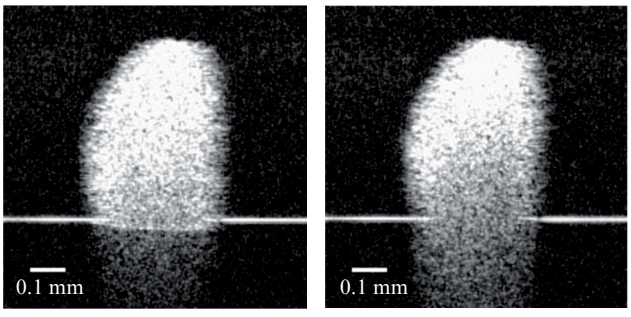

Figure 10. OCT images of a secondary tendon bundle sample obtained with incident radiation polarisation (a) perpendicular and (b) parallel to the direction of the fibrils.

In general, the results of the experiment performed allow us to assert that the theoretical model described in Section 2 is adequate and provides good prediction accuracy, at least with respect to the relative change in $\mu_{s\perp}$ with decreasing c_w and the location of the upper boundary of the range of c_w values, where $\mu_{s||}$ and $\mu_{s\perp}$ are very small.

Thus, an experimental verification of the adequacy of a simple theoretical model for assessing the optical characteristics of collagen bundles at various levels of tissue hydration was carried out. The presented experimental data give reason to believe that this model is suitable and reflects well the changes in the optical properties of collagen bundles during their dehydration.

Acknowledgements. The experimental part of the work was supported by the Russian Foundation for Basic Research (Grant No. 19-32-90177), and the theoretical part was supported by the Russian Science Foundation (Project No. 19-12-00118).

References

1. Sinichkin Yu.P., Uts S.R. *In vivo otrazhatel'naya i fluorestsentnaya spektroskopiya kozhi cheloveka* (In Vivo Reflection and Fluorescence Spectroscopy of Human Skin) (Saratov: Saratov University Press, 2001).
2. Kirillin M.Y., Agrba P.D., Kamensky V.A. *J. Biophotonics*, **3** (12), 752 (2010).
3. Ermakov I.V., Gellermann W. *J. Biophotonics*, **5** (7), 559 (2012).
4. Yanina I.Yu. et al. *Proc. SPIE*, **11641**, 116410W (2021).
5. Yakovlev D.D., Sagaidachnaya E.A., Yakovlev D.A., Kochubey V.I. *Quantum Electron.*, **51** (1), 43 (2021) [*Kvantovaya Elektron.*, **51** (1), 43 (2021)].
6. Rylander C.G. et al. *J. Biomed. Opt.*, **11** (4), 041117 (2006).
7. Tuchin V.V. *Optical Clearing of Tissues and Blood* (Bellingham, WA, USA: SPIE Press, 2005).
8. Starborg T. et al. *Nat. Protoc.*, **8** (7), 1433 (2013).
9. Jones P.N. *Connective Tissue Research*, **26** (1–2), 11 (1991).
10. Hovhannisyan V. et al. *J. Biomed. Opt.*, **18** (4), 046004 (2013).
11. Meek K.M. et al. *Biophys. J.*, **60** (2), 467 (1991).
12. Morin C., Hellmich C., Henits P. *J. Theor. Biology*, **317**, 384 (2013).
13. Hayes S. et al. *J. Royal Society Interface*, **14** (131), 20170062 (2017).
14. Shvachkina M.E. Cand. Sci. Thesis (Saratov, Saratov State University, 2020).
15. Schmitt J.M., Kumar G. *Appl. Opt.*, **37** (13), 2788 (1998).
16. Twersky V. *J. Opt. Soc. Am.*, **65** (5), 524 (1975).
17. Bohren C.F., Huffman D.R. *Absorption and Scattering of Light by Small Particles* (New York: Wiley, 1983).
18. Daimon M., Masumura A. *Appl. Opt.*, **46** (18), 3811 (2007).
19. Shvachkina M.E., Yakovlev D.D., Pravdin A.B., Yakovlev D.A. *J. Biomed. Photonics & Engineering*, **4** (1), 010302 (2018).
20. Shvachkina M.E., Yakovlev D.D., Lazareva E.N., Pravdin A.B., Yakovlev D.A. *Opt. Spectrosc.*, **127** (2), 359 (2019) [*Opt. Spektrosk.*, **127** (2), 337 (2019)].
21. Martinez-Anton J.C., Bernabeu E. *Thin Solid Films*, **313**, 85 (1998).

22. De Aro A.A., de Campos Vidal B., Pimentel E.R. *Micron*, **43** (2), 205 (2012).
23. Kastelic J., Galeski A., Baer E. *Connective Tissue Research*, **6** (1), 11 (1978).
24. Rowe R.W.D. *Connective Tissue Research*, **14** (1), 9 (1985).
25. Kannus P. *Scand. J. of Medicine and Science in Sports*, **10** (6), 312 (2000).
26. Screen H.R.C. et al. *Acta Biomater.*, **2** (5), 505 (2006).
27. Gong P. et al. *J. Biomed. Opt.*, **25** (4), 040901 (2020).
28. Van Leeuwen T.G., Faber D.J., Aalders M.C. *IEEE J. Sel. Top. Quantum Electron.*, **9** (2), 227 (2003).
29. Yun S.H. et al. *Opt. Express*, **11** (26), 3598 (2003).
30. Gerrard A., Burch J.M. *Introduction to Matrix Methods in Optics* (Mineola, NY: Dover Publications, 2012).
31. Faber D.J., van der Meer F.J., Aalders M.C.G., van Leeuwen T.G. *Opt. Express*, **12** (19), 4353 (2004).
32. Thrane L., Yura H.T., Andersen P.E. *J. Opt. Soc. Am. A*, **17** (3), 484 (2000).
33. Turchin I.V., Sergeeva E.A., Dolin L.S., Kamensky V.A. *Laser Phys.*, **13** (12), 1524 (2003).
34. Almasian M. et al. *J. Biomed. Opt.*, **20** (12), 121314 (2015).
35. Aernouts B., van Beers R., Watté R., Lammertyn J., Saeys W. *Opt. Express*, **22** (5), 6086 (2014).
36. Yadlowsky M.J., Schmitt J.M., Bonner R.F. *Appl. Opt.*, **34** (25), 5699 (1995).